SAND2019-14871J

SHAPE-CONSTRAINED INPUT ESTIMATION FOR EFFICIENT MULTI-SHAKER VIBRATION TESTING

R. Schultz[1,2], P. Avitabile[1]

[1] Department of Mechanical Engineering, University of Massachusetts Lowell, 1 University Avenue, Lowell, MA 01854, USA

[2] Sandia National Laboratories, 1515 Eubank Blvd. SE, Albuquerque, NM 87123

ABSTRACT

Multi-shaker vibration testing is gaining interest from structural dynamics test engineers as it can provide a much more accurate match to complicated field vibration responses than traditional single-axis shaker tests. However, the force capabilities of the small modal shakers typically used in multi-shaker vibration tests has limited the achievable response levels. To date, most multi-shaker vibration tests have been performed using a variety of standard, commercially-available control systems. While these control systems are adequate for a wide range of multiple-input/multiple-output tests, their control algorithms have not been tailored for the specific problem of multi-shaker vibration tests: efficiently coordinating the various shakers to work together to achieve a desired response. Here, a new input estimation algorithm is developed and demonstrated using simulations and actual test data. This algorithm, dubbed shape-constrained input estimation, is shown to effectively coordinate multiple shakers using a set of constraint vectors based on the deflection shapes of the test structure. This is accomplished by using the singular vector shapes of the system frequency response matrix, which allows the constraint vectors to automatically change as a function of frequency. Simulation and test results indicate a significant reduction in the input forces required to achieve a desired

response. The results indicate that shape-constrained input estimation is an effective method to achieve higher response levels from limited shaker forces which will enable higher level multi-shaker vibration tests to be performed.

1 INTRODUCTION

Laboratory vibration testing is used to subject aerospace structures to vibration environments to assess their performance to complex field environments including acoustic or aeroacoustic loads. Traditionally, single-axis shakers have been used to subject a device under test (DUT) to a vibration environment. However, this type of base shake input is often not representative of the field load paths and boundary conditions, which results in inaccurate vibration response of the DUT. Recently, multi-shaker vibration test methods have been used to improve controllability in laboratory vibration testing [1, 2, 3, 4]. These techniques utilize a multiple-input/multiple-output (MIMO) controller to control several small modal shakers distributed about the DUT, resulting in accurate control of the vibration response at many points on the DUT over a wide frequency range. However, the limited force capability of these shakers imposes a limitation on the achievable response levels from the multi-shaker test technique. This paper introduces shape-constrained input estimation as a new technique for effectively coordinating multiple shakers to achieve higher response levels from a given input force level. This technique essentially matches the shaker inputs to the dominant mode shapes of the DUT at each frequency line, ensuring that the shaker forces efficiently excite the DUT.

MIMO testing has been used for several years to improve the response accuracy of laboratory vibration tests. There are essentially two types of MIMO laboratory vibration tests: six degree of freedom tests and multi-shaker tests. In six degree of freedom testing, a DUT is attached to a shaker table which can vibrate in all six degrees of freedom [5]. In multi-shaker testing, several shakers are distributed around a DUT which is typically suspended in a free-free configuration bare or via an impedance-matching fixture [3, 6, 7]. Multi-shaker vibration testing of this kind began with the work of Daborn, Ind, and Ewins [2]. The concept of using multiple, distributed shaker inputs was later exercised using a mock missile DUT with a multiple-input/multiple-output (MIMO) controller to match response from a field environment in a wind tunnel [6]. Others have utilized the multi-shaker concept to test other DUTs with different types of field environment responses, such as direct-field and reverberant acoustic environments [1, 3].

To date, commercial MIMO control systems have been utilized to determine the shaker inputs. However, Daborn introduced a modification to the typical MIMO control problem with the so-called buzz test approach wherein the cross-terms of the target field responses are replaced with the coherence and phase of the lab DUT subject to uncorrelated inputs [8]. While this technique inherently changes the target response cross-terms, it does generally improve the accuracy of the response auto-power spectral densities (APSDs). Another example of a modified control technique used in multi-shaker testing comes from Mayes and Rohe where an independent drives approach was used to generate uncorrelated shaker inputs [3]. In this technique, the inputs are defined to be uncorrelated and estimated to match only the APSDs. Both these techniques have elements of the independent drives method from Smallwood [9], where the control

problem is first solved assuming independent inputs, predicting the response due to those independent inputs and using that predicted response as a new target cross-power spectral density (CPSD) matrix.

These methods all modify the control equations to change how the inputs are estimated. In this work, a new modification is made to the input estimation equation to improve the coordination between multiple shaker inputs which enables higher response levels to be achieved from a given input level. This modification utilizes a set of constraints based on the singular value decomposition of the system frequency response function (FRF) matrix and essentially allows the shakers to better approximate the significant mode shapes in the DUT response.

2 THEORETICAL BACKGROUND

MIMO linear systems can be characterized by an FRF matrix which relates the outputs to the inputs. In the context of random vibration, outputs and inputs are often defined in terms of a CPSD matrix. This form enables ensemble averaging, reducing the effects of noise, and allows for accurate estimates of the inputs and outputs to be obtained. This averaging necessitates a change from the linear-space MIMO equation:

$$\{X_y\} = [H]\{X_x\} \tag{1}$$

to a power-space MIMO equation:

$$[S_{yy}] = [H][S_{xx}][H]^H , \tag{2}$$

where $\{X_x\},\{X_y\}$ are the linear spectra of the inputs and outputs. $[S_{xx}],[S_{yy}]$ are the MxM and NxN CPSD matrices of the inputs and outputs, $[H]$ is the MxN FRF matrix, and the superscript $[\square]^H$ denotes a conjugate transpose, or Hermitian of the FRF matrix. Note that this is viewing the equation at a single frequency line, and in practice this equation is evaluated on a frequency line by frequency line basis. Equation 2 is valid for single input or single output cases; in that case the M or N dimension is simply equal to one. More outputs or more inputs make the FRF matrix more rectangular in the row or column dimensions, respectively. If the number of inputs exceeds the number of outputs, the solutions is not a least squares solution, although this is typically not an issue in practice where the number of outputs is usually larger than the number of inputs. In general, it is advisable to use more outputs than inputs, as this enables a least-squares form of the input estimation problem:

$$[S_{xx}] = [H]^{+}[S_{yy}][H]^{+H}, \tag{3}$$

where the superscript $[\square]^{+}$ denotes the pseudo-inverse of the FRF matrix and $[S_{xx}]$ is now the estimate of the required inputs given the system FRF matrix and a target response $[S_{yy}]$. Often the target responses come from field measurements, though they could be from a specification or otherwise derived.

Note that the inputs from this standard MIMO input estimation approach are the inputs which cause the laboratory response CPSD matrix to best match the field response CPSD matrix in a least-squares sense. That is, the estimated inputs, $[S_{xx}]$, will provide a

response CPSD matrix which most closely matches the entire target CPSD matrix, not just the APSDs but all the cross-terms as well. However, typically the response APSD is of primary concern and the cross-terms are disregarded and thus, while the inputs are estimated to match the cross-terms, the energy required to do so is essentially wasted.

2.1 SHAPE-CONSTRAINED INPUT ESTIMATION

Modification of the input estimation method can change the response accuracy or required inputs. Here, the objective is to improve the efficiency, or output given some input, in MIMO, multi-shaker tests. Shape-constrained input estimation was developed based on the generality that at any frequency line there are just a small number of active, significant modal responses which dictate the total response of a DUT. By constraining multiple shaker inputs to resemble a set of modes which are active in the response, those modes can be strongly excited from a set of shaker forces. The concept is intuitive and in fact has been used for many years in the context of forced normal modes testing [10, 11]. However, in forced normal modes testing the objective is to coordinate the shakers to achieve single-mode response for measurement of that mode, whereas in MIMO vibration testing the objective is to coordinate the shakers to efficiently excite a small number of modes which accurately match a target response.

Implementation of shape-constrained input estimation begins by multiplying the FRF matrix by a constraint matrix, $[C]$:

$$\left[\hat{S}_{xx}\right] = \left[[H][C]\right]^{+}\left[S_{yy}\right]\left[[H][C]\right]^{+H} \quad . \tag{4}$$

Note the estimated inputs here are $\left[\hat{S}_{xx}\right]$. These are not the actual shaker inputs but are a set of $\hat{N}$ inputs where $\hat{N}$ is the number of vectors in the constraint matrix. Conversion to the full set of N inputs is done with:

$$\left[S_{xx}\right] = \left[C\right]\left[\hat{S}_{xx}\right]\left[C\right]^{H} \quad . \tag{5}$$

Effectiveness of this new input estimation method relies on the content of $\left[C\right]$. Intuitively, at a well-isolated peak in the response near the i-th mode frequency, a constraint matrix containing a single constraint vector equal to the i-th mode shape, $\left\{U_i\right\}$, should effectively coordinate the various shakers and efficiently drive the response. In that case $\left[C\right]$ is N by 1 and therefore $\left[\hat{S}_{xx}\right]$ is 1 by 1. All N inputs are therefore fixed to the shape of $\left\{U_i\right\}$. Consider a second case at a frequency line between two modes. In that case, the response is likely due to a combination of two or more modes. There, multiple constraint vectors would be required to allow the response to be accurately replicated. If just a single mode shape is used as a constraint, but the response is due to a combination of several mode shapes, the response will not match exactly. Additionally, the response is due to a different mode or set of modes at different frequencies. At low frequency, the response is mainly due to the lower modes but at higher frequency the response is due to higher modes.

Thus, a methodology is needed to choose different vectors to populate the constraint matrix, $\left[C\right]$, at each frequency line. While mode vectors could be exchanged at each frequency line, this would require the user to select which mode or modes to use at

each frequency line. Here, the approach is to use right singular vectors of the FRF matrix in place of mode shapes. Replacing mode shapes with right singular vectors has the advantage of automatically varying with frequency because the singular vectors change as the FRF matrix changes. The right singular vectors change as a function of frequency because the singular value decomposition of the FRF matrix can be performed at each frequency line as:

$$[H] = [U_\Sigma][S_\Sigma][V_\Sigma]^H \ , \tag{6}$$

where the left and right singular vector matrices are the complex, unitary matrices $[U_\Sigma], [V_\Sigma]$ respectively and $[S_\Sigma]$ is a matrix with singular values on the diagonal. The left singular vectors represent the shapes at the output degrees of freedom and the right singular vectors represent the shapes at the input degrees of freedom [12].

Singular vectors work as constraint shapes because they resemble the mode shapes. As an example, near a resonant frequency, the dominant singular vector will be very similar to the mode shape. To demonstrate this, a beam model was created. Details of this model are presented in the next section but characteristics of this model are shown here for demonstration. This fixed-free beam is subject to four point force inputs at different locations down the length of the beam. The mode shapes of the beam are compared with the right singular vectors at these four input locations in Figure 1. As the singular vectors are complex-valued, the signed magnitude is shown for simplicity. For each of the three modes shown in Figure 1, the right singular vectors very closely resemble the mode shapes.

Figure 2 shows the process of extracting constraint shapes from the FRF matrix. This begins by forming the MxN FRF matrix of the DUT with M responses at the gauge locations and N inputs at the shaker locations. Next, the singular value decomposition is used to extract the singular values and singular vectors of the FRF matrix at each frequency line. The matrix of right singular vectors, $[V_\Sigma]$, contains N singular vectors, $\{V_1\},\{V_2\}...\{V_N\}$. One or more of those vectors can then be used as constraint shapes in the constraint matrix. These vectors or shapes change as a function of frequency, as shown on the right-hand side of Figure 2 where the four right singular vectors are plotted at two frequency lines, 20 Hz and 124 Hz. These two frequencies correspond to the first two mode frequencies of the beam and as such the top singular vectors strongly resemble the mode shapes at those frequency lines and the other singular vectors resemble combinations of other adjacent modes.

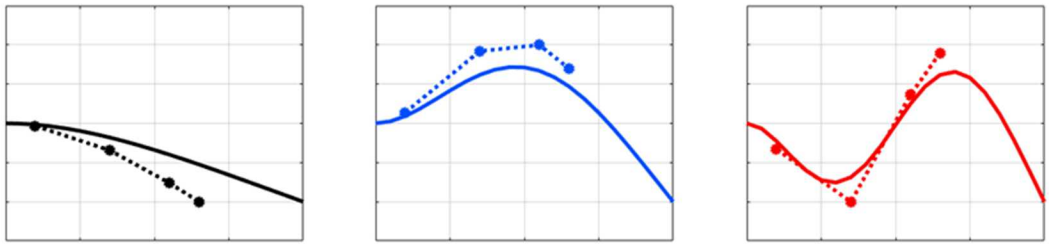

Figure 1: Comparison of mode shapes (solid) and right singular vectors (dotted) for the first three modes of a fixed-free beam

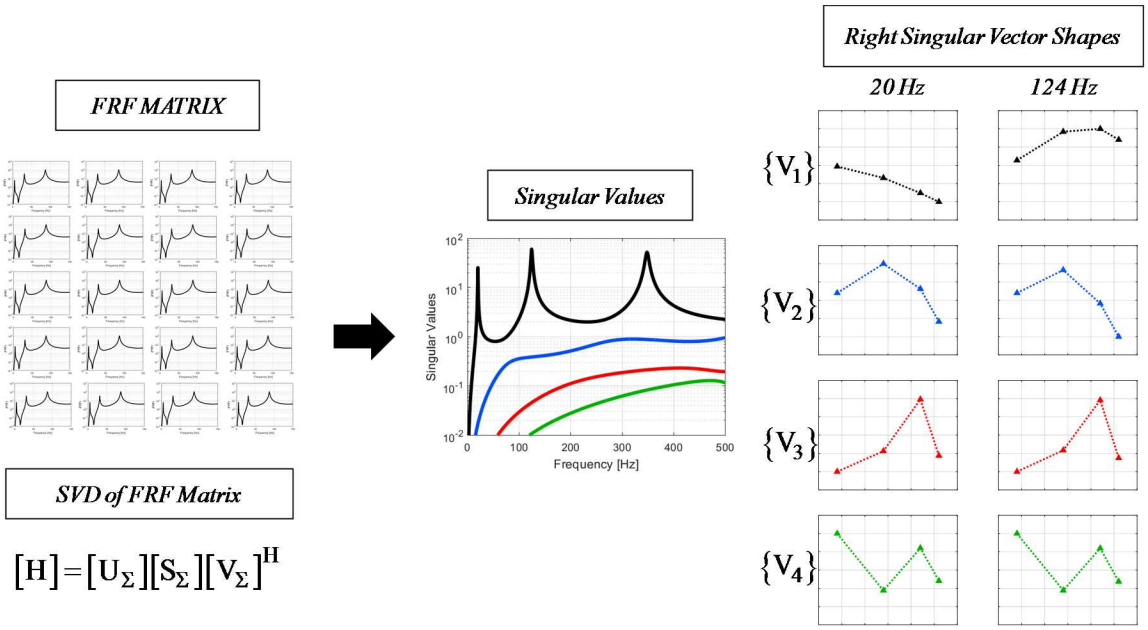

Figure 2: Diagram of the process of extracting right singular vector constraint shapes from the system FRF matrix

To further demonstrate how singular vectors resemble mode shapes, two cases are examined in Figure 3 and Figure 4. At a chosen frequency line, the singular vectors associated with the largest and second largest singular values are plotted along with the mode shape or shapes nearest that frequency line. Figure 3 shows the singular vectors at the frequency of mode 1. As this frequency is right at the mode frequency, the largest singular vector shape closely resembles the mode shape. Figure 4 shows the singular vector shapes at a frequency between two modes, mode 1 and mode 2. Here, the singular vectors are a combination of the two significant mode shapes at that frequency, a blend of the shapes of mode 1 and mode 2.

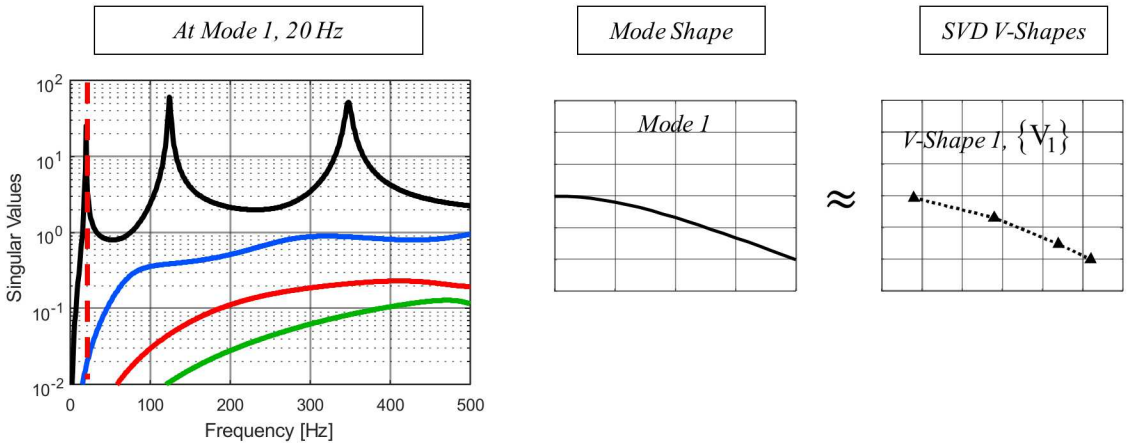

$$[H] = [U_\Sigma][S_\Sigma][V_\Sigma]^H$$
$$[V_\Sigma] = \left[\{V_1\}\{V_2\}\{V_3\}\{V_4\}\right]$$

Figure 3: Largest two singular vector shapes at a frequency near mode 1

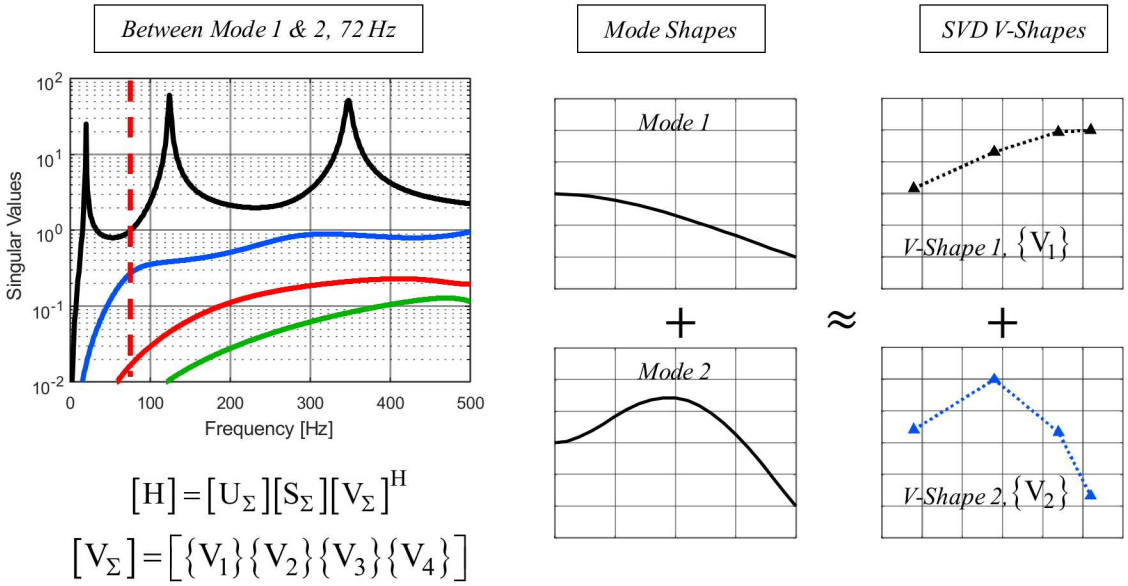

$$[H] = [U_\Sigma][S_\Sigma][V_\Sigma]^H$$
$$[V_\Sigma] = \left[\{V_1\}\{V_2\}\{V_3\}\{V_4\}\right]$$

Figure 4: Largest two singular vector shapes at a frequency between mode 1 and 2

Populating the constraint matrix with right singular vectors has some interesting consequences. For one, because singular vectors are orthogonal, the multiplication of the FRF matrix with the constraint matrix results in a rank-reduced form of the FRF matrix. This can be seen by writing out the FRF matrix in terms of the singular value decomposition and then multiplying by a constraint matrix consisting of two singular vectors, for example:

$$[H][C] = [U_\Sigma][S_\Sigma][V_\Sigma]^H \left[\{V_1\}\{V_2\}\right] . \tag{7}$$

The multiplication of the Hermitian of the right singular vector matrix with a matrix of two singular vectors results in a constrained FRF matrix, $\left[[H][C]\right]$, with rank two. In effect, using right singular vectors as constraints removes the contributions of the other singular values. All other singular values are effectively set to zero due to the orthogonality between singular vectors.

As such, shape-constrained input estimation is an extreme form of regularization. Regularization is often used to reduce numerical errors in input estimation problems [13, 14, 15]. A common technique is Tikhonov regularization wherein small changes are made to the FRF matrix, affecting all singular values and reducing the negative effects of small singular values. Another approach is to perform the singular value decomposition on the FRF matrix and then modify the small singular values by making them larger or setting them to zero. Setting them to zero is called rank reduction, which is exactly what is occurring when using right singular vectors as constraint shapes in shape-constrained input estimation. Typically, regularization aims to only affect the very smallest singular values in a matrix to preserve the overall form of the matrix as much as possible. In

contrast, in shape-constrained input estimation a small number of constraint vectors are used, thereby zeroing out all but the very largest singular values in the FRF matrix.

2.2 AUTOMATIC VECTOR SELECTION

Choosing the number of singular vectors to use in the constraint matrix can be user-specified. For example, the largest two singular vectors could be used at every frequency line. However, response near resonances is usually dominated by a single mode, which corresponds to a single large singular value, so using two vectors is not ideal at those frequency lines and more efficiency can be achieved by using just a single constraint vector. Conversely, between resonances the response is typically a combination of multiple modes. In that case, better accuracy can be achieved by using multiple constraint vectors. To address this, an automatic vector selection algorithm was developed to automatically determine the number of vectors to use in the constraint matrix of shape-constrained input estimation. This algorithm proceeds as follows at each frequency line. First, the singular values of the FRF matrix are computed. Next, the singular values are normalized with respect to the largest singular value. Then, a threshold value is specified for these normalized singular values. This threshold value is chosen by the test engineer and can be set to a higher or lower value to achieve specific test results. Finally, the number of constraint vectors is chosen by the number of normalized singular values above that threshold value. This effectively chooses the number of constraint vectors based on the number of “large” singular values, with “large” determined by the threshold value.

Figure 5 shows an example FRF from the beam FRF matrix along with the singular values of the FRF matrix to show how near the mode frequencies there is generally a single dominant singular value, but between modes there are two or more significant singular values. Intuitively, near a mode frequency, the pattern of the inputs should match that mode shape. In terms of constraint vectors, this means that near a mode frequency, there should just be a single constraint vector representing the largest singular value resulting in a singular vector shape which closely resembles the mode shape. Between mode frequencies, the desired input pattern is a combination of mode shapes and can best be accomplished by using two or more singular vectors.

The original and normalized singular values are shown in Figure 5. For example, a threshold value of 0.2 is chosen and shown in the dotted line of the normalized singular values plot. This means that at a given frequency line, the number of constraint vectors is equal to the number of normalized singular values above 0.2 of the largest singular value. Figure 6 shows the number of singular values above two different threshold values, 0.05 and 0.2. For some frequency lines, there is just one large singular value and thus just a single constraint vector should be used. For other frequency lines, there are two, three or four large singular values and two, three or four constraint vectors should be used. A larger threshold value results in fewer constraint vectors as there are fewer singular values above that higher threshold. Thus, modifying the threshold value allows the test engineer to change the constraints in the input estimation process, changing the balance between inputs and responses.

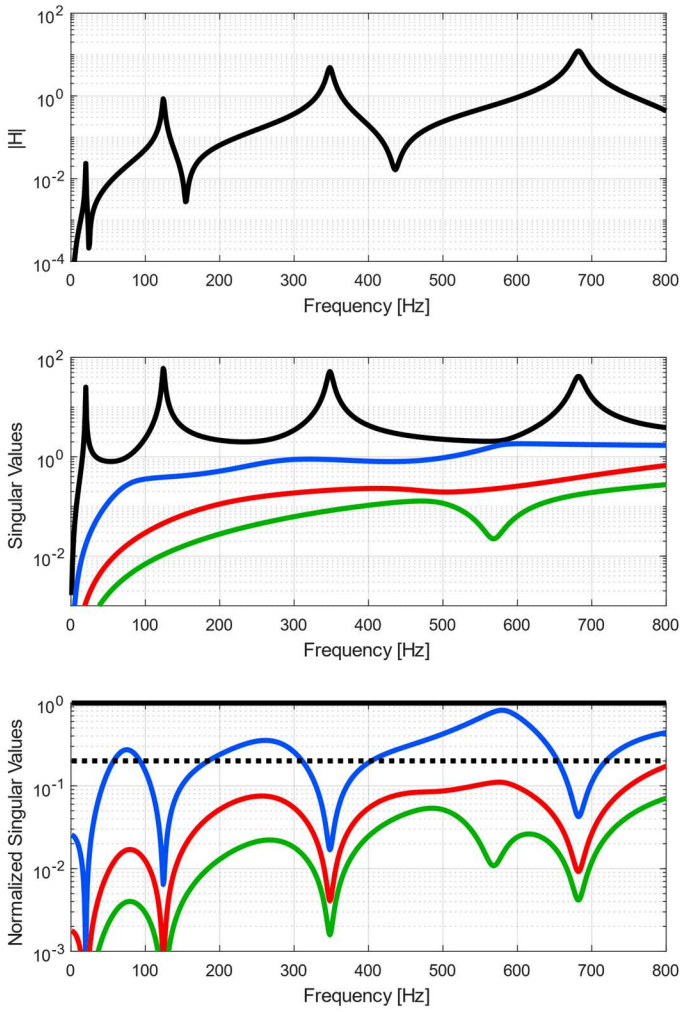

Figure 5: Overlay of an example FRF (top) with the singular values of the FRF matrix (middle) and the singular values normalized to the largest singular value with a 0.2 threshold value shown with a dotted line (bottom)

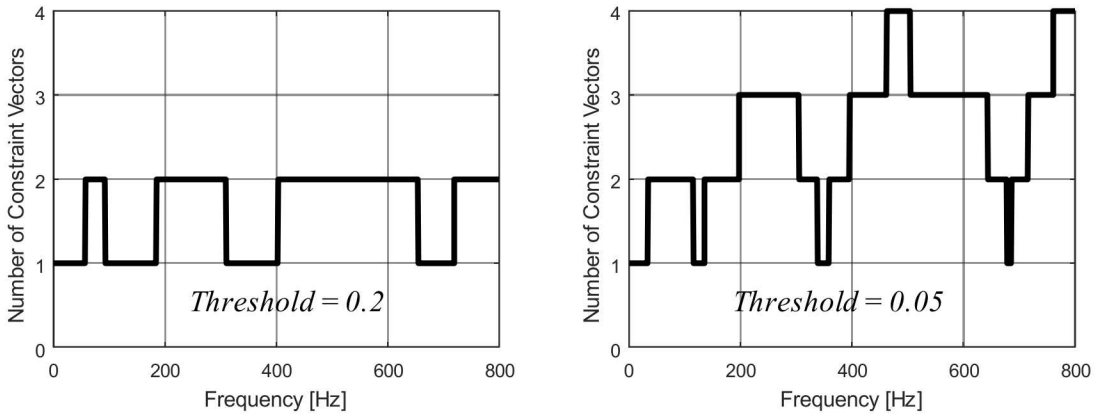

Figure 6: Number of constraint vectors chosen by the automatic vector selection algorithm

3 DEMONSTRATION OF SHAPE-CONSTRAINED INPUT ESTIMATION USING A BEAM SUBJECT TO POINT FORCES

The first demonstration of shape-constrained input estimation uses a beam model comprised of 20 elements, 21 nodes and fixed-free boundary conditions. The beam model is 1 inch wide by 1 inch thick and 40 inches long and has aluminum material properties. First, the beam is subjected to some field environment which provides the CPSD matrix of target responses. Next, those target responses are used to estimate inputs to the beam in the laboratory configuration, which in this case simply means that there are inputs at different locations than the field configuration. In the field configuration, there are 2 point force inputs, at nodes 6 and 18. In the laboratory configuration, there are 4 point force inputs, at nodes 3, 8, 12, and 14 as shown in Figure 7. Responses are captured in either configuration at 5 nodes 4, 6, 9, 10, and 19. These input and output locations were chosen arbitrarily and simply result in a system with more outputs than inputs and

different input locations in the laboratory configuration compared with the field configuration.

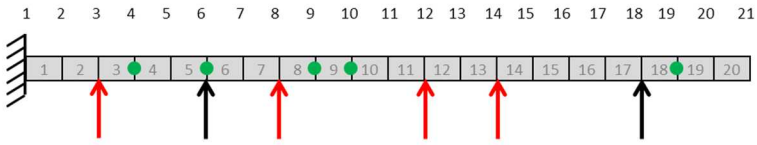

Figure 7: Beam model with 5 output locations (green dots), 2 field input locations (black arrows) and 4 laboratory input locations (red arrows)

A field environment is simulated using uniform uncorrelated forces with APSD levels of 0.01 lbf^2/Hz from 0 to 800 Hz at each of the two field input locations. This results in a field, or target, response at the five output locations. Next, the target response CPSD matrix is used to estimate the four laboratory input forces using both standard and shape-constrained input estimation. The automatic vector selection algorithm is used to determine the number of constraint vectors based on a threshold value of 0.2. The singular values of the 5x4 laboratory FRF matrix are shown in Figure 5 and the number of constraint vectors chosen by the automatic vector selection algorithm is shown in Figure 6. The threshold value of 0.2 is appropriate here as it allows for a single constraint vector near the well-isolated peaks in the FRF and allows two or more vectors at frequencies between the peaks. This low modal density frequency range means the response is largely dominated by single mode response. This is demonstrated by plotting the sum of the response APSDs in terms of the modal contributions in Figure 8. As expected, at each peak, the response is due to just a single mode. Between peaks, the response is due to a combination of two or more modes.

The laboratory inputs are determined using standard and shape-constrained input estimation methods and the resulting response is computed from the estimated inputs. This results in a 4x4 input CPSD matrix and a 5x5 output CPSD matrix. Rather than plot the CPSD matrices in their entirety which would be difficult to view and make useful comparisons, the APSD information in those matrices is shown two ways, each condensing the data down in either the spatial or frequency dimension. First, the input and response APSDs are condensed in the spatial dimension by taking the sum over all inputs or responses, which is the trace of the CPSD matrix. Second, the APSDs are condensed in the frequency dimension by computing the root mean square (RMS) of the inputs and responses. These two metrics for inputs and responses are shown in Figure 9. The four-input laboratory responses are compared with the two-input field, target response. The response using either the standard or shape-constrained input estimation methods largely matches the target response, with only minor discrepancies in the regions between peaks. Standard input estimation is slightly more accurate than shape-constrained input estimation, though the overall differences are minimal. However, standard input estimation requires considerably higher input forces over the entire bandwidth. The RMS force in this case is reduced by at least 1.3 times, as in shaker 1 (2.07 vs. 2.82 lbf), and as much as 7.7 times, as in shaker 3 (1.65 vs. 12.77 lbf), by using shape-constrained input estimation instead of standard input estimation. This simple beam model with point force inputs demonstrates how shape-constrained input estimation can be used to effectively replicate a target response while significantly reducing the required input forces.

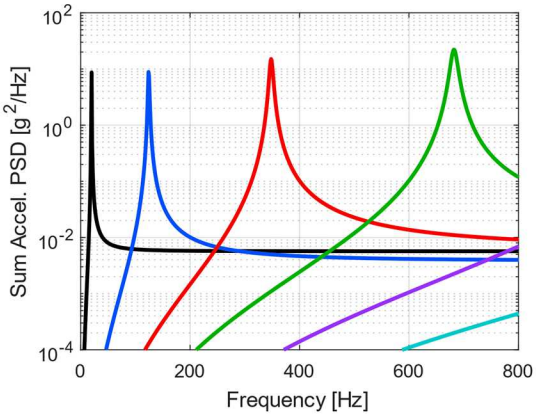

Figure 8: Target response PSD shown in terms of mode contributions with response due to each mode shown in a different color

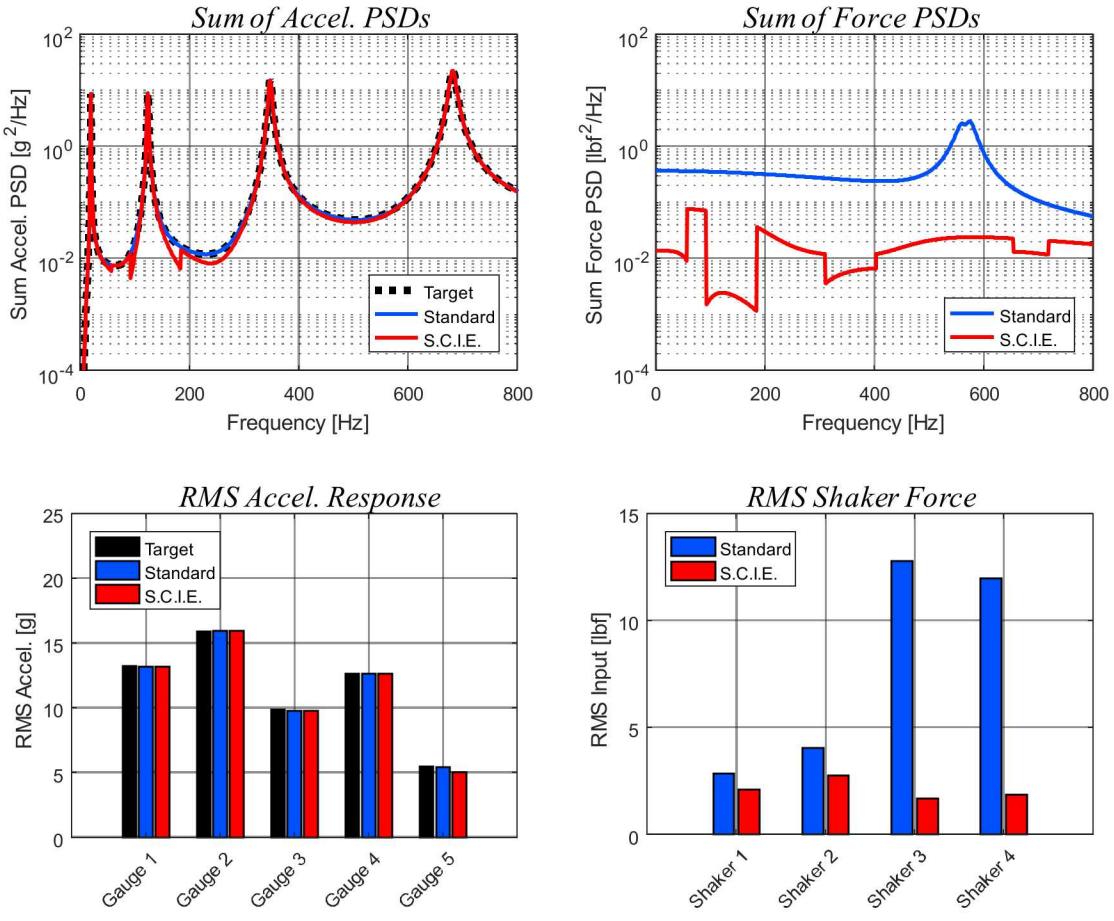

Figure 9: Response and input comparing standard and shape-constrained input estimation (S.C.I.E.) applied to the beam model

4 DEMONSTRATION OF SHAPE-CONSTRAINED INPUT ESTIMATION USING A PLATE SUBJECT TO A DISTRIBUTED PRESSURE

The second demonstration of shape-constrained input estimation uses a model of a 12 inch by 24 inch by 0.25 inch aluminum plate. This model uses one inch by one inch shell elements to capture the transverse displacement. To increase complexity of the field environment over the beam example from the previous section, the field forces are defined as the acoustic pressure of a uniform diffuse field. The diffuse field has a distribution of pressure over the surface of the plate with frequency-dependent spatial correlation, meaning the relationship between pressure at different points on the structure is a function of the distance between the points and the excitation frequency [16, 17]. This type of acoustic pressure loading is common in vibroacoustic testing and provides a complicated set of field environment loads that should be difficult to fully replicate with a small number of point force inputs representing shakers in a laboratory configuration. The laboratory configuration consists of either four or eight point forces on the plate as shown in Figure 10. In both the field and laboratory configurations, the response is measured at the 20 locations shown in Figure 10. In this example, these locations were chosen with the effective independence method, but any good sensor selection method could have been utilized [18].

A uniform diffuse pressure load is applied with constant amplitude for all frequencies between 500 and 1000 Hz, resulting in an overall sound pressure level of 130 dB, referenced to 20 micro-Pascals. The frequency range of 500 to 1000 Hz was chosen as it contains both well-isolated and closely-spaced modes. The pressures are converted to forces at all the nodes on the plate model and applied as a force CPSD matrix to the

FRF matrix of the plate to obtain the field, target response. This simulated field response is then used to explore the effects of shape-constrained input estimation in various ways, including the effects of the number of inputs, the number of constraint vectors and the automatic vector selection threshold value.

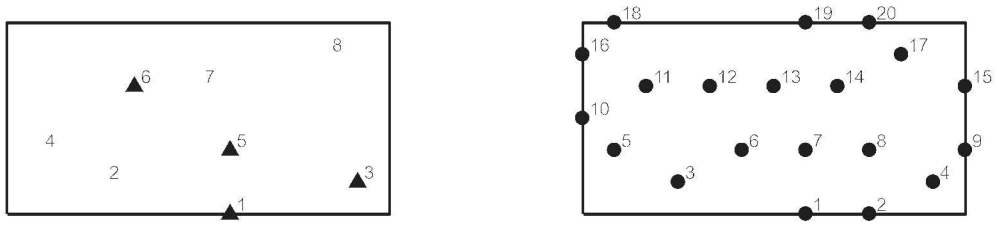

Figure 10: Eight shaker locations, with the subset of four shown in red (left) and 20 gauge locations (right) shown on the plate model

First, a four-shaker configuration is simulated. These four inputs are located at the red triangles in the left side of Figure 10, at input locations 2, 4, 7, and 8. While these input locations could be chosen with some optimization routine, here they were chosen simply to be independent in terms of the modes in the bandwidth. Input forces for these shakers in the laboratory configuration were then estimated using standard and shape-constrained input estimation methods using all 20 accelerometers in the target response CPSD matrix. The shape-constrained input estimation case uses the automatic vector selection algorithm with a threshold value of 0.5 to choose the number of singular vector constraints at each frequency line. The resulting input forces and responses are shown in Figure 11 in terms of the sum of acceleration and force PSDs and the RMS acceleration

and force. For brevity, a selection of three gauges, 5, 10, and 15, are shown in the response RMS acceleration plot. In contrast to the beam example where there were just two discrete field loads, the distributed pressure field loads used in this simulation results in a response which cannot be perfectly replicated by the four shakers in the laboratory configuration. Response is matched well at the peaks, but not as well between peaks. Thus, a small number of shakers is capable of replicating response where a single mode is dominant in the response, but not capable of matching at frequencies between peaks where the response is due to a more complicated combination of multiple modes. Shape-constrained input estimation performs nearly as well as standard input estimation in terms of matching the field response, with the only difference being at the low-response regions between peaks. The input force is again significantly reduced with shape-constrained input estimation, in this case the mean reduction in RMS force is 46 percent with shaker 2 having the largest reduction in RMS force at 54 percent.

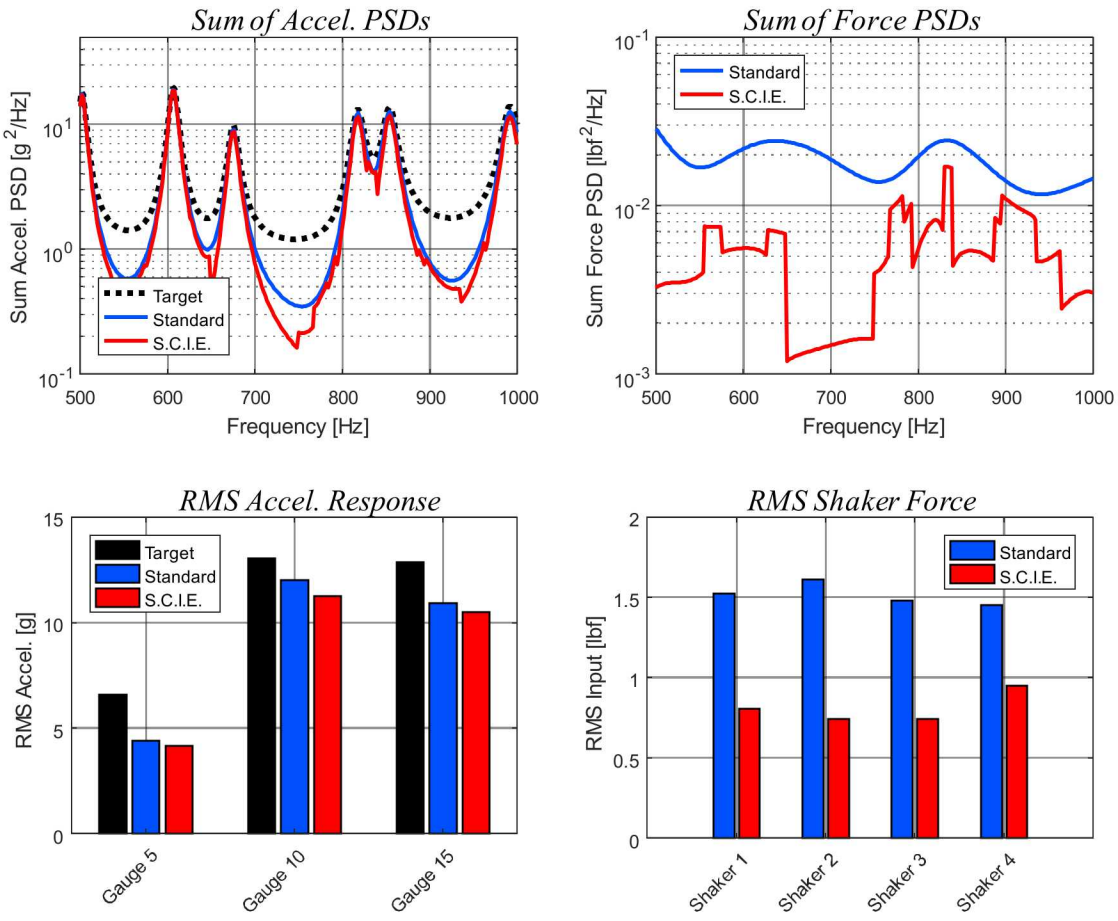

Figure 11: Responses and inputs comparing standard and shape-constrained input estimation (S.C.I.E.) for four shakers on the plate model

The quality of replication of the cross-terms in the CPSD matrix is also of interest. Figure 12 shows the coherence and CPSD magnitude for one pair of gauges, gauge 1 and 2. As four shakers are not sufficient to fully replicate the APSDs, they are also insufficient to accurately replicate the cross-terms. Application of constraints effectively reduces the controllable space, which results in slightly poorer accuracy in these cross-terms. In fact, if a single constraint vector is used, the coherence is unity for all cross-terms because there is just a single input to the linear system. This can be seen at

several frequencies in the bandwidth, including at 700 Hz where the coherence is unity because a single constraint vector was used, fully correlating all four shaker inputs.

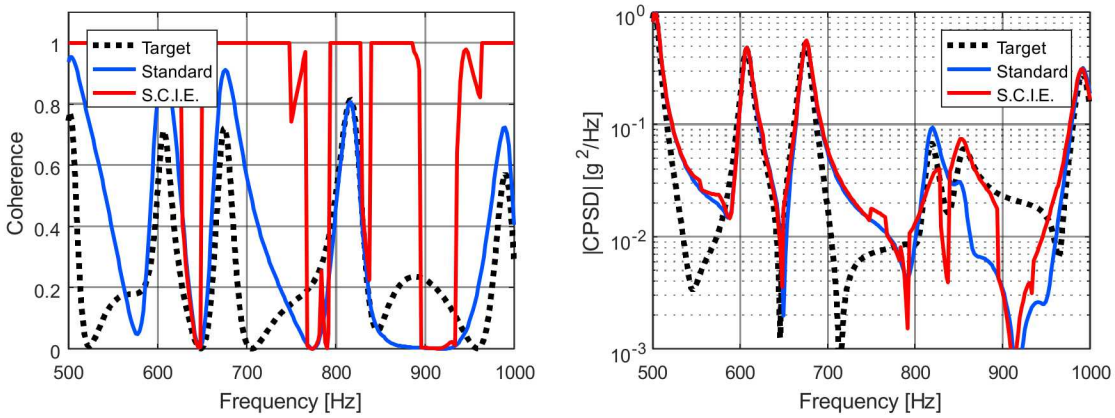

Figure 12: Resulting cross-terms of the response of two gauges shown as coherence (left) and CPSD magnitude (right) comparing standard and shape-constrained input estimation (S.C.I.E.) for four shakers on the plate model

Next, the number of shakers is increased from four to eight to examine how increasing the number of inputs affects response accuracy and input force requirements. Increasing the number of inputs increases the size of the controllable space, which should result in a better match to the field response. Figure 13 shows the response and inputs which result when using eight shakers. As expected, with more shakers the match to the target response improves, particularly when using standard input estimation. The improvement in response accuracy is not as strong when using shape-constrained input estimation because the constraints applied to the FRF matrix effectively reduce the controllable space. However, this reduction in controllable space is only important between peaks; at the peaks either input estimation technique accurately matches the response.

Interestingly, when using the standard input estimation method, the shaker forces actually increase when using eight shakers instead of four shakers. This is because the controllable space is larger with eight shakers than with four shakers, meaning the laboratory response CPSD can be more accurately matched to the target CPSD. However, this improved match to the target response CPSD matrix comes at the cost of higher shaker forces, thus the use of shape-constrained input estimation results in an even more dramatic reduction in the required input forces when more shakers are added. Here with eight shakers instead of four, the RMS force using shape-constrained input estimation is 80 percent lower, on average, than when using standard input estimation. The greatest reduction in input is at shaker 3 with a 92 percent reduction in RMS force and the smallest reduction in input is at shaker 1 with a 55 percent reduction. This effectively means that with the same shaker equipment, a test using shape-constrained input estimation could be run at 12 dB higher levels than a test using standard input estimation, assuming that input force is the main limiting factor. This also demonstrates how shape-constrained input estimation is especially useful when a large number of shakers is used in a multi-shaker test.

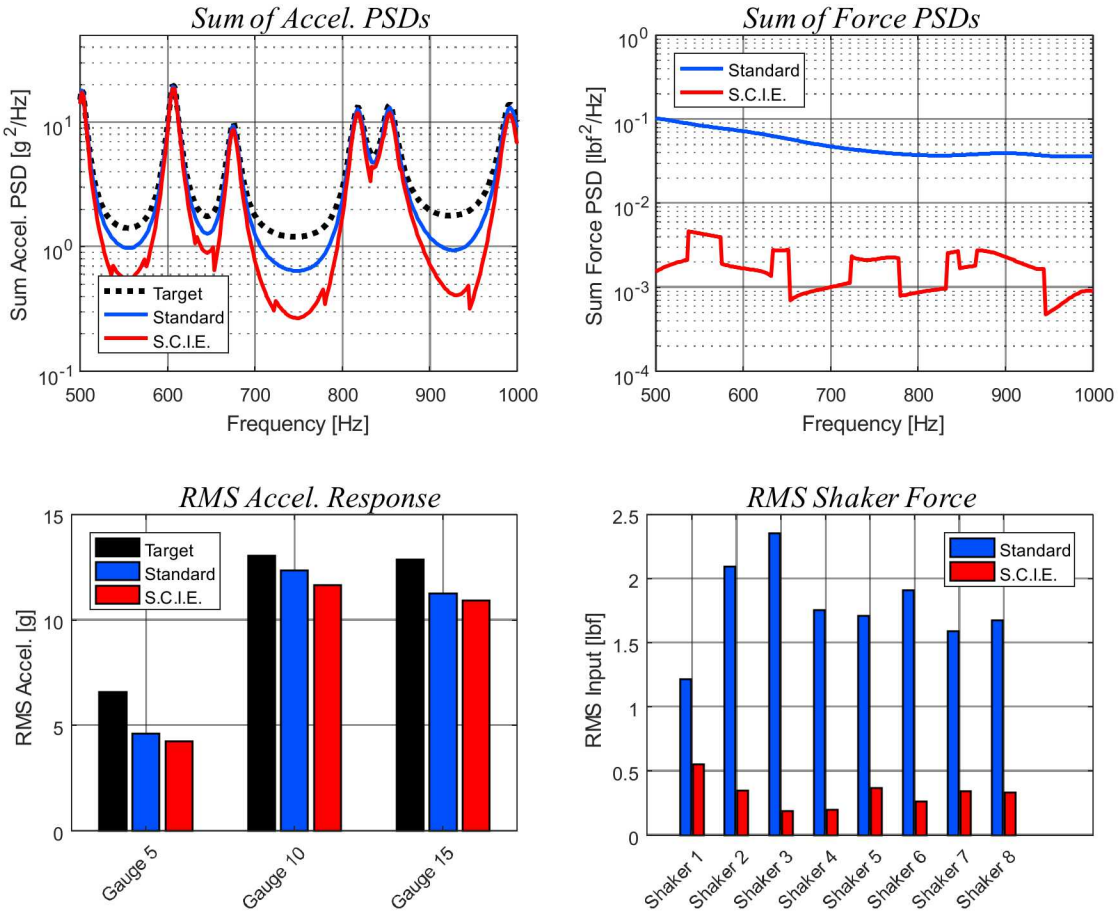

Figure 13: Responses and inputs comparing standard and shape-constrained input estimation (S.C.I.E.) for eight shakers on the plate model

The effects of the number of constraint vectors is also of interest. So far, all simulations have utilized the automatic vector selection algorithm. Here, the number of vectors is fixed at one, two, or three constraint vectors for all frequency lines to examine how the number of constraint vectors affects response accuracy and input force requirements. Figure 14 shows the response and inputs which result from estimating inputs to four shakers with a constant one, two, or three constraint vectors. There is a consistent trend of higher response accuracy with more constraint vectors, although the

differences only exist between peaks in the response. At the peaks, all cases are the same. There is also a consistent trend in the input forces, with more force required as more constraint vectors are used. This clearly demonstrates how there is a balance between response accuracy and input force when choosing the number of constraint vectors to use in shape-constrained input estimation.

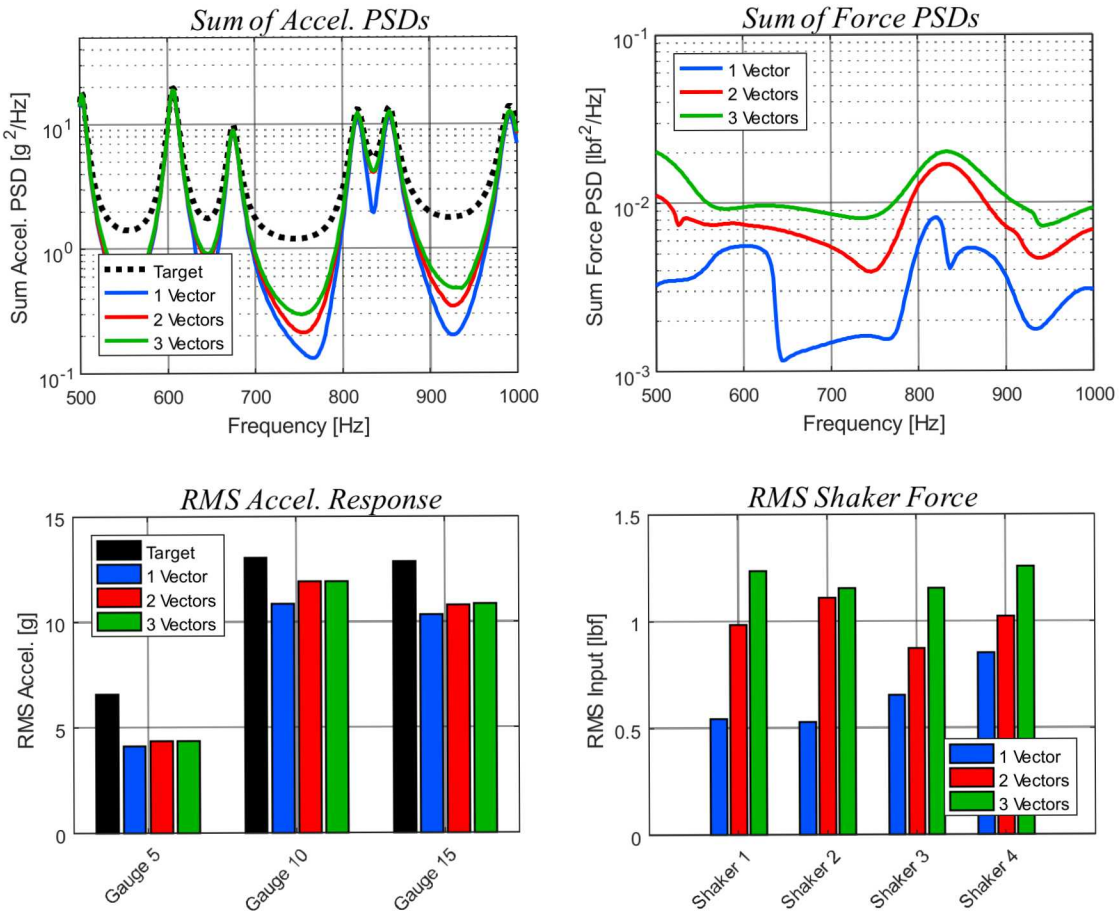

Figure 14: Responses and inputs comparing shape-constrained input estimation using a constant of one, two, or three constraint vectors for all frequency lines

The automatic vector selection algorithm was developed to automatically choose the number of constraint vectors to use based on the structure of the FRF matrix at each frequency line. In this way, more constraint vectors can be used between peaks in the response, where multiple modes combine in the response, and just a single constraint vector can be used at the peaks in the response, where there is just a single dominant mode. The test engineer can use the threshold value to balance response accuracy and input force when using the automatic vector selection algorithm. To demonstrate this, two threshold values were used in simulation of the four-shaker configuration of the plate model. Figure 15 shows the singular values of the plate model FRF matrix, normalized to the largest singular value. Two threshold values, 0.2 and 0.5 are shown in dotted lines. The number of constraint vectors chosen is shown in the right plot of Figure 15, and indicates the number of singular values above those threshold values. A threshold value of 0.2 results in several frequency lines with three or four constraints where a threshold value of 0.5 results just one constraint for many frequency lines.

Figure 16 shows the response and inputs with the two different threshold values. The lower threshold value results in slightly improved response accuracy, because the controllable space is larger. However, this results in increased force requirements as shown in the plots of RMS force and sum of force PSDs. As such, the threshold value provides a simple, effective tool for the test engineer to balance requirements of a specific test, resulting in improved response accuracy or reduced input forces by simply changing the threshold value.

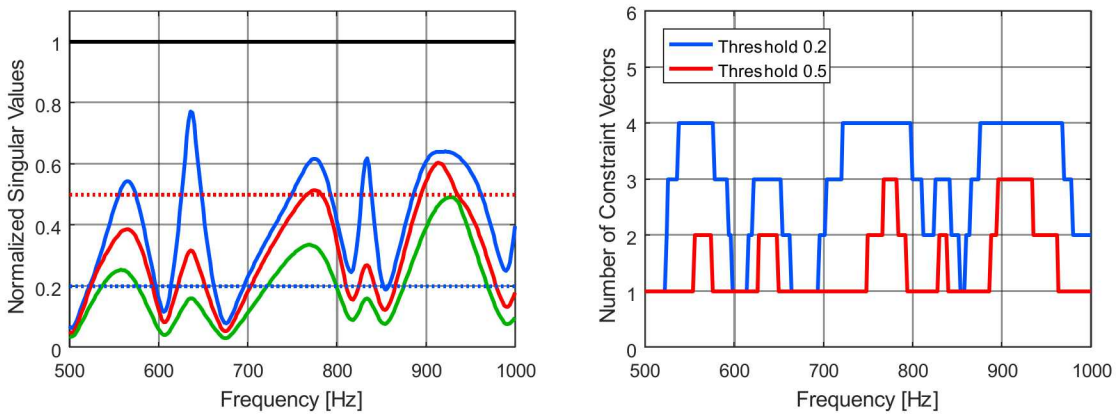

Figure 15: Normalized singular values showing the two threshold values (left) and number of singular values above the threshold value, indicating the number of constraint vectors (right)

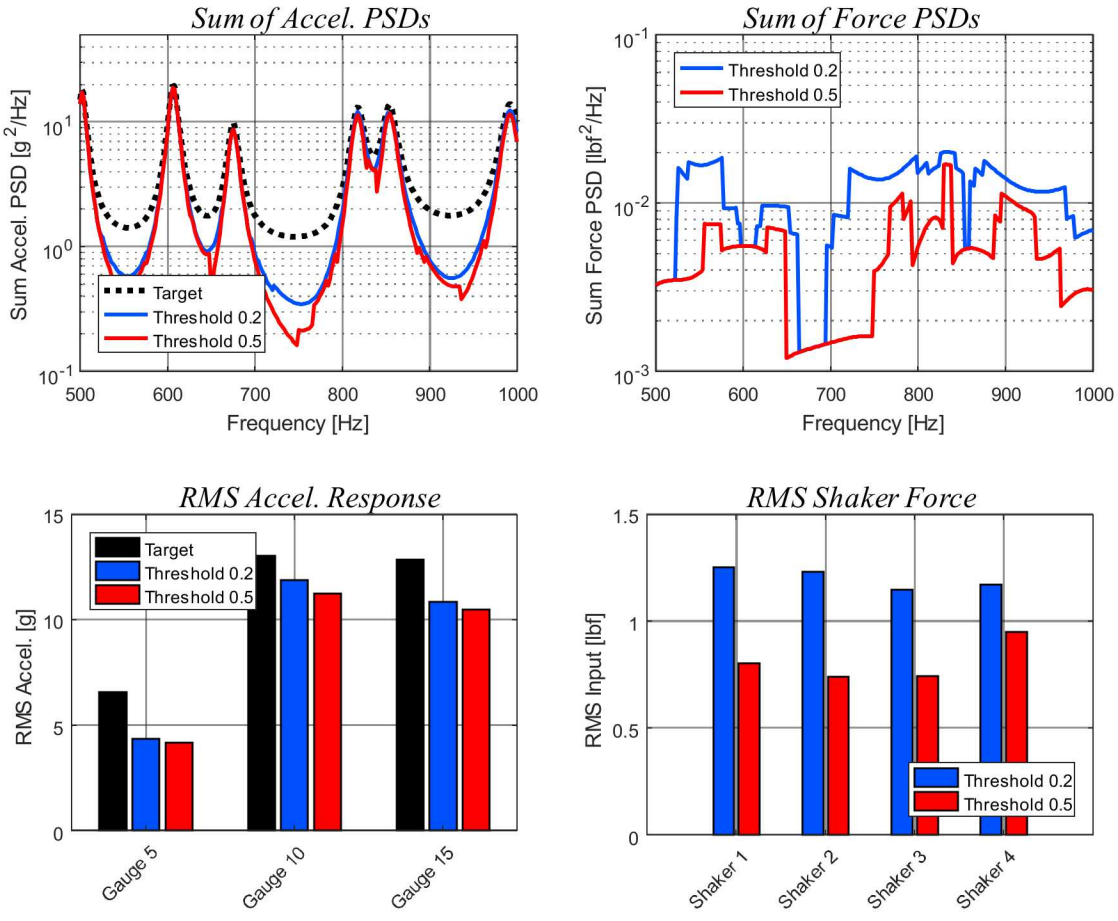

Figure 16: Responses and inputs comparing two different automatic vector selection algorithm threshold values

5 IMPLEMENTATION IN A LABORATORY TEST

Simulations of MIMO input estimation problems using the beam and plate models demonstrate the general behavior of shape-constrained input estimation and how it compares to standard input estimation. Next, both input estimation techniques were utilized in a laboratory experiment. In this experiment, a 12 inch by 24 inch by 0.25 inch aluminum plate DUT was suspended via bungees from a frame. Accelerometers measured the transverse vibration at each of the 20 locations shown in Figure 10. Three small modal shakers were attached to the plate through load cells at three arbitrary locations. While the location of shakers is important, optimization of their locations was not part of the current study. As the plate DUT is small and light, the effects of affixing shakers affects the dynamics of the DUT, so the shakers were left attached for all experiments to maintain consistent DUT dynamics. An array of 24 loudspeakers were arranged around the plate to provide acoustic excitation for the field test. Three independent inputs were sent to eight loudspeakers each using band-limited white noise between 100 and 2000 Hz. The input voltage level and speaker amplifier gain was set such that a 0.8 volt-RMS input signal resulted in an overall sound pressure level of 118 dB. The acoustic environment caused response of the plate with an average RMS response of 0.4 g. Time histories of the accelerometer signals were captured and used to compute the field, or target, CPSD matrix.

A customizable open-loop MIMO controller was developed to enable implementation of the shape-constrained input estimation technique. This controller takes time history input and response data, computes CPSD and FRF matrices, and solves the input estimation problem using user-specified techniques and settings. The estimated input

CPSD matrix is transformed into voltage time histories using signal synthesis techniques which are described in several papers [19, 20, 21].

Next, the FRF matrix of the laboratory configuration was determined by inputting white noise inputs to the three shakers. This acceleration/voltage FRF matrix was then used to estimate shaker inputs using standard and shape-constrained methods. The automatic vector selection algorithm provided the frequency-dependent constraint vectors used in the shape-constrained method. The resulting response shown in Figure 18 largely agrees with the plate simulation results. Response is matched well at most of the peaks using either method, meaning either method matches the majority of the response energy. Standard input estimation is somewhat more accurate between peaks, consistent with the simulation results. Based on the observations of simulations using multiple inputs to match response from point force or acoustic loads, it would be expected that a better match to the response over the entire bandwidth would be achieved if the target response came from point force inputs instead of the more complicated loads imparted by the direct field acoustic input used here. Input voltage and input force also follow the simulation trends, as seen in Figure 19 and Figure 20. Both force and voltage were reduced over much of the frequency range when using shape-constrained input estimation. The RMS input levels were reduced by 10, 33, and 50 percent for shakers 1, 2, and 3, respectively. Overall, the experiment qualitatively agrees with the simulation results, and demonstrates that shape-constrained input estimation can be used to reduce input levels for MIMO vibration tests.

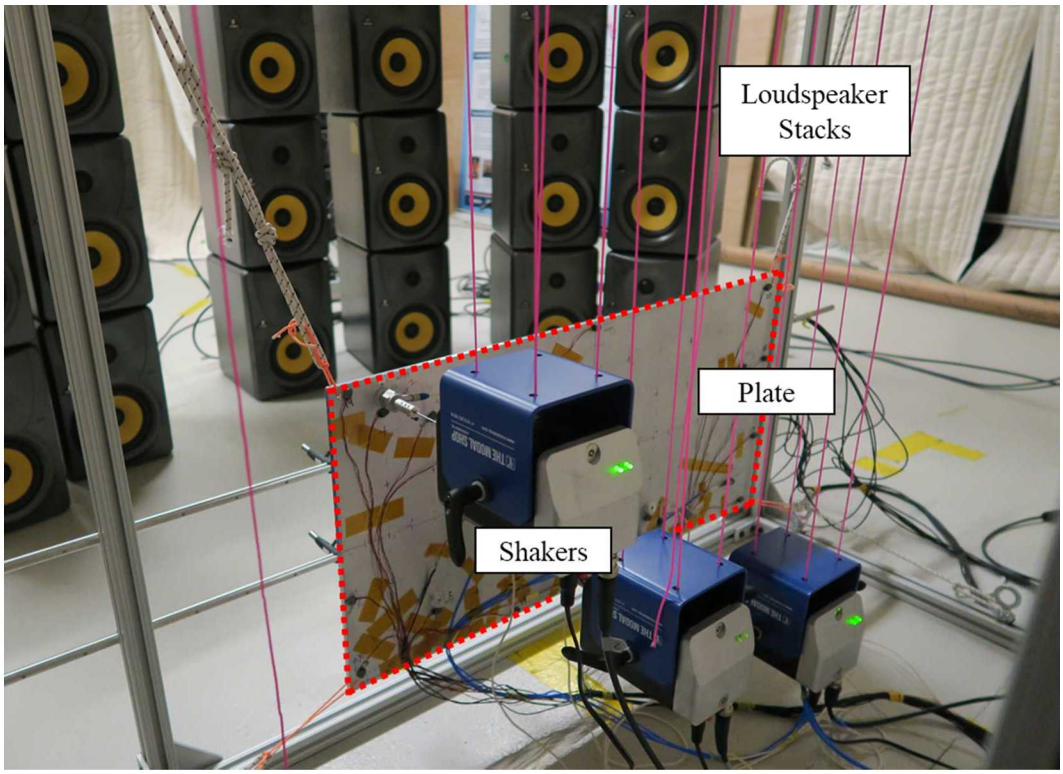

Figure 17: Test setup with the plate and shakers suspended from a frame surrounded by stacks of loudspeakers

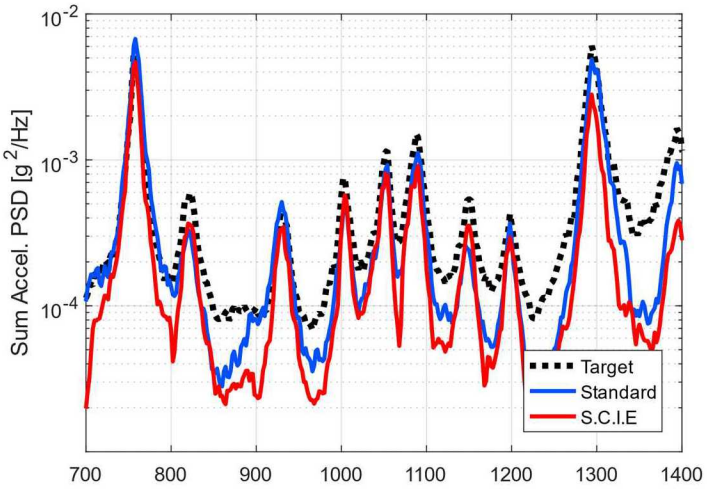

Figure 18: Response of the plate in terms of the sum of all accelerometer APSDs comparing the truth response with shaker replica tests using standard and shape-constrained input estimation.

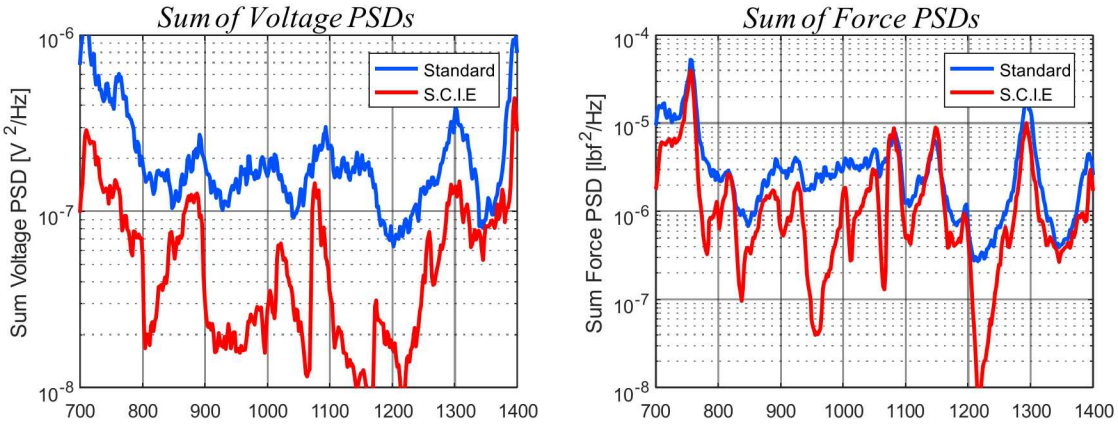

Figure 19: Shaker input APSDs comparing standard and shape-constrained input estimation. Left: Voltage APSD. Right: Force APSD.

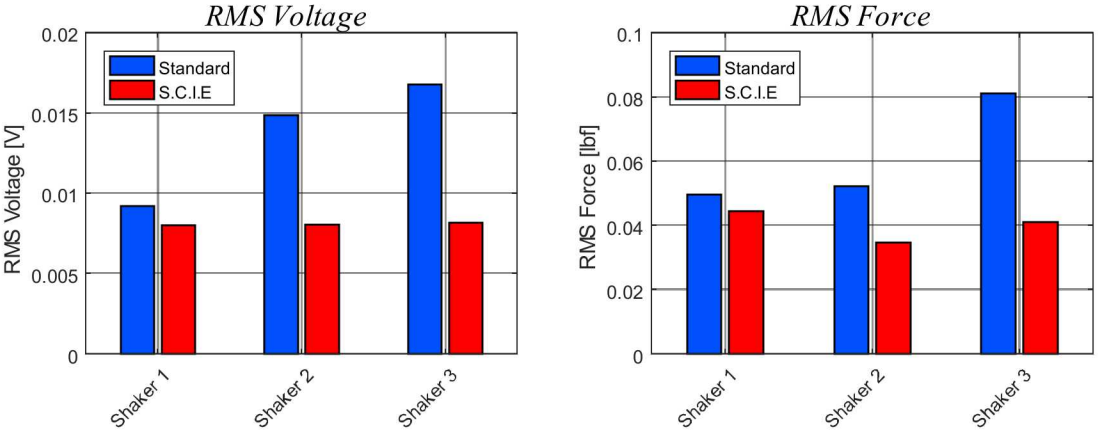

Figure 20: RMS drive voltage (left) and shaker force (right) comparing standard and shape-constrained input estimation.

6 CONCLUSIONS

While multi-shaker vibration testing can provide improved response accuracy compared with traditional single-axis test techniques, the limited force capabilities of the small modal shakers typically used in these tests limits the achievable response levels. Shape-

constrained input estimation provides an elegant solution to this problem, utilizing the right singular vectors of the DUT system FRF as a set constraint vectors. These constraint vectors coordinate shakers together, resulting in higher response levels. An algorithm was presented to automatically determine the number of constraint vectors to use at each frequency line based on the content in the FRF matrix, and the user can easily balance response accuracy and input force by changing the threshold value. These techniques were compared with standard input estimation in simulations of two different DUT models and also in a multi-shaker experiment. In all cases, shape-constrained input estimation was shown to provide nearly as accurate response replication and significantly reduced inputs. By reducing the required inputs, this technique has promise in increasing the achievable response levels of multi-shaker vibration tests.

ACKNOWLEDGEMENTS

Sandia National Laboratories is a multimission laboratory managed and operated by National Technology & Engineering Solutions of Sandia, LLC, a wholly owned subsidiary of Honeywell International Inc., for the U.S. Department of Energy's National Nuclear Security Administration under contract DE-NA0003525. This paper describes objective technical results and analysis. Any subjective views or opinions that might be expressed in the paper do not necessarily represent the views of the U.S. Department of Energy or the United States Government. On behalf of all authors, the corresponding author states that there is no conflict of interest.

REFERENCES

[1] P. M. Daborn, "Scaling up of the Impedance-Matched Multi-Axis Test (IMMAT) Technique," in *Proceedings of IMAC XXXV, the 35th International Modal Analysis Conference*, Garden Grove, CA, 2017.

[2] P. M. Daborn, P. R. Ind and D. J. Ewins, "Replicating aerodynamic excitation in the laboratory," in *Proceedings of IMACXXXI, the 31st International Modal Analysis Conference*, 2013.

[3] R. L. Mayes and D. P. Rohe, "Physical Vibration Simulation of an Acoustic Environment with Six Shakers on an Industrial Structure," in *Proceedings of IMACXXIV, the 34th International Modal Analysis Conference*, 2016.

[4] C. Roberts and D. J. Ewins, "Multi-axis vibration testing of an aerodynamically excited structure," *Journal of Vibration and Control,* vol. 24, no. 2, pp. 427-437, 2018.

[5] M. A. Underwood and M. Hale, "MIMO testing methodologies," in *Proceedings of the 79th Shock and Vibration Symposium*, 2008.

[6] P. M. Daborn, C. Roberts, D. J. Ewins and P. R. Ind, "Next-generation random vibration tests," in *IMAC XXXII, the 32nd International Modal Analysis Conference*, Orlando, FL, 2014.

[7] D. P. Rohe, G. D. Nelson and R. Schultz, "Strategies for shaker placement for impedance-matched multi-axis testing," in *Proceedings of IMAC XXXVII, the 37th International Modal Analysis Conference*, 2019.

[8] P. M. Daborn, "Smarter Dynamic Testing of Critical Structures," PhD Thesis, University of Bristol, 2014.

[9] D. O. Smallwood, "A proposed method to generate a spectral density matrix for a multiple input, multiple output (MIMO) vibration test," in *Proceedings of the 81st Shock and Vibration Symposium*, Orlando, FL, 2010.

[10] J. R. Wright, J. E. Cooper and M. J. Desforges, "Normal-mode force appropriation - theory and application," *Mechanical Systems and Signal Processing,* vol. 12, no. 2, pp. 217-240, 1999.

[11] C. D. Van Karsen, K. P. Wittrup and J. P. DeClerck, "The application of stepped sine and normal mode testing to automotive structures," in *Proceedings of IMACXIV, the 14th International Modal Analysis Conference*, 1996.

[12] J. B. Fahnline, R. L. Campbell, S. A. Hambrick and M. R. Shepherd, "Modal analysis using the singular value decomposition and rational fraction polynomials," The Applied Research Laboratory, The Pennsylvania State University, State College, PA, 2017.

[13] P. C. Hansen, Discrete inverse problems: Insight and Algorithms, SIAM: the Society for Industrial and Applied Mathematics, 2010.

[14] H. G. Choi, A. N. Thite and D. J. Thompson, "Comparison of methods for parameter selection in Tikhonov regularization with applicate to inverse force determination," *Journal of Sound and Vibration,* vol. 304, pp. 894-917, 2007.

[15] R. Schultz, "A demonstration of force estimation and regularization methods for multi-shaker testing," in *Proceedings of IMAC XXXVII, the 37th International Modal Analysis Conference*, 2019.

[16] F. Jacobsen, "The diffuse sound field," Acoustics Laboratory at the Technical University of Denmark, 1979.

[17] M. Kuster, "Spatial correlation and coherence in reverberant acoustic fields: Extension to microphones with arbitrary first-order directivity," *The Journal of the Acoustical Society of America,* vol. 123, no. 1, 2008.

[18] D. C. Kammer, "Sensor placement for on-orbit modal identification and correlation of large space structures," *Journal of Guidance, Control, and Dynamics,* vol. 14, no. 2, pp. 251-259, 1991.

[19] D. O. Smallwood, "Multiple shaker random control with cross coupling," in *Proceedings of the Institute of Environmental Sciences*, 1978.

[20] D. O. Smallwood and T. L. Paez, "A frequency domain method for the generation of partially coherent normal stationary time domain signals," *Shock and Vibration,* vol. 1, no. 1, 1991.

[21] R. Schultz and G. D. Nelson, "Input signal synthesis for open-loop multiple-input/multiple-output testing," in *Proceedings of IMAC XXXVII, the 37th International Modal Analysis Conference*, 2019.